Kim *et al. Earth, Planets and Space* (2023) 75:113
https://doi.org/10.1186/s40623-023-01864-x

Earth, Planets and Space

FULL PAPER

Joint inversion of ocean-bottom pressure and GNSS data from the 2003 Tokachi-oki earthquake

SatByul Kim[1], Tatsuhiko Saito[2], Tatsuya Kubota[2] and Sung-Joon Chang[3*]

Abstract
When the 2003 Tokachi-oki earthquake generated a large tsunami off eastern Hokkaido, Japan, it was detected by cabled ocean-bottom pressure gauges (OBPs) installed within the seismic source region. The OBP records included characteristic features of tsunami waveforms in the source region, indicating significant offset due to the permanent sea-bottom displacement, which can provide critical information about the earthquake source. However, no studies have considered the OBP tsunami data observed in the focal region for the source inversion of the Tokachi-oki earthquake. Here, in order to better understand the 2003 Tokachi-oki earthquake source, we estimate the spatial distribution of fault slip by conducting a joint inversion using two different datasets: tsunami data from four OBPs, located in the focal region and about 300 km away to the south, as well as Global Navigation Satellite System (GNSS) data obtained throughout Hokkaido and northern Honshu. Through our joint inversion, we found that the most dominant slip peak is located 40 km northwest from the hypocenter with an abnormally large slip of ~15 m. This large slip may result from releasing a high amount of slip deficit accumulated by a stick–slip patch surrounded by stable slip regions on the southernmost Kuril subduction zone. By comparing the OBP observations and the synthetic tsunami waveforms derived from our fault model and other fault models, we conclude that the OBP tsunami data recorded within the focal region better constrained the magnitude and the location of the slip compared to other geophysical data.

Keywords The 2003 Tokachi-oki earthquake, Ocean-bottom pressure gauges, Tsunami, Geodetic data, Joint inversion

*Correspondence:
Sung-Joon Chang
sjchang@kangwon.ac.kr
Full list of author information is available at the end of the article

Graphical Abstract

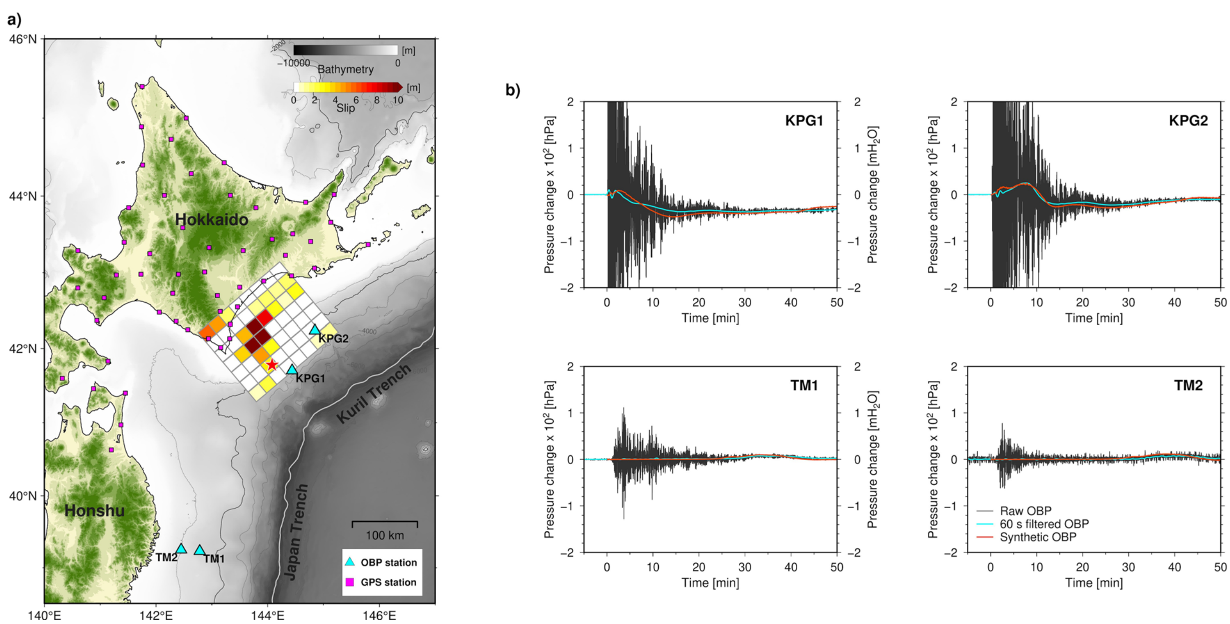

Introduction

The 2003 Tokachi-oki earthquake occurred on 26 September 2003 off the coast of eastern Hokkaido, Japan, in the southern region of the Kuril subduction zone (Fig. 1a) and caused widespread damage along the eastern Hokkaido coast with tsunami heights as large as 4 m in some places (Tanioka et al. 2005). This region has experienced large tsunamigenic earthquakes at intervals of roughly 450 years during the past 4000 years (e.g., Nanayama et al. 2003, 2007) due to the subduction of the Pacific plate beneath the North American plate. The ruptures of the earthquakes occurring here typically consist of three subregions, which are the Tokachi-oki, Akkeshi-oki, and Nemuro-oki regions (Satake et al. 2005b). For example, one of the earliest tsunamis for which observations were written in historical documents occurred in 1843, when an M8 earthquake ruptured in the Akkeshi-oki region as determined from tsunami heights (Fig. 1a; Satake et al. 2005b). Nearly 100 years later, another M8 earthquake occurred in 1952 that ruptured the Tokachi-oki and Akkeshi-oki regions (Hirata et al. 2003, 2007; Satake et al. 2006; Kobayashi et al. 2021). This earthquake was initiated close to the epicenter of the 2003 event, but it ruptured a wider region (Hirata et al. 2004). This 1952 event also caused tsunamis with a maximum tsunami run-up of approximately 7 m along the coast between Kushiro and Akkeshi region (Tanioka et al. 2004c). In the Nemuro-oki region, the latest tsunamigenic earthquakes occurred in 1894 and 1973 (Tanioka et al. 2007). Their tsunamis were mostly observed along the coasts of Akkeshi and Nemuro, and the tsunami heights were larger on the eastern coast of southeast Hokkaido (Satake 2017).

Since the recurrence time of large earthquakes in the southernmost region of the Kuril trench is rather short given the size of the earthquakes that have occurred, researchers had anticipated that another earthquake would occur in the southern Kuril subduction zone, which indeed happened in 2003. Low earthquake activities had been found in the Tokachi-oki region and this region was pointed out as a potential location for the next large earthquake (Motoya 1999; Ichiyanagi et al. 2003). In 1999, the Japan Agency for Marine-Earth Science and Technology (JAMSTEC) built a permanent and real-time cable-connected seismic observatory system including ocean-bottom pressure gauges (OBPs) and seismometers (OBS) on the deep seafloor off Hokkaido to monitor earthquakes, tsunamis, and other geophysical phenomena (Hirata et al. 2002). It was the first time a large subduction zone earthquake (M8 class) was recorded right above the source region (Watanabe et al. 2004). The 2003 Tokachi-oki earthquake was recorded at those new systems and was also recorded at Global Navigation Satellite System (GNSS) observation stations, tide gauges, and global and local seismic stations.

Many studies have been conducted to estimate the slip distribution of the 2003 Tokachi-oki earthquake by

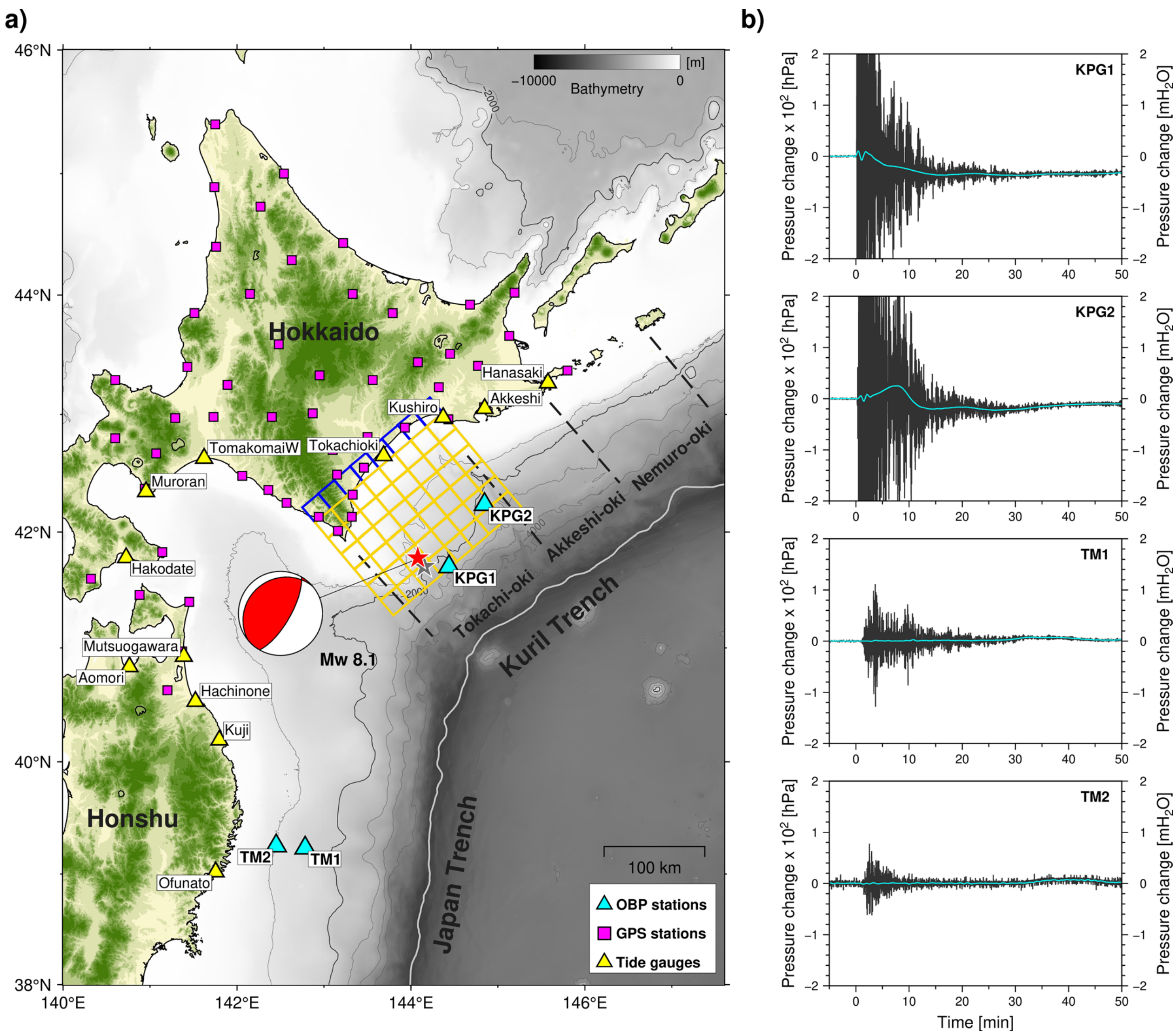

Fig. 1 **a** Map of the epicentral region of the 2003 Tokachi-oki earthquake and locations of OBP gauges and GNSS stations that are used for the joint inversions, and tide gauges used in tsunami simulation. The epicenter of the 2003 Tokachi-oki earthquake is marked as a red star. The gray star indicates the epicenter of the 1952 Tokachi-oki earthquake. The focal mechanism solution is from Yamanaka and Kikuchi (2003). The subfaults displayed as yellow lines are taken from Tanioka et al. (2004a) and the blue lines are newly extended fault portions in this study. The dark gray dashed lines indicate the rupture subregions (Satake et al. 2005b). **b** Observed tsunami records at the four OBP stations. The black lines are OBP records after removing the tide effect and the cyan lines show tsunami signals after applying a low-pass filter and converting to a pressure unit of mH_2O

inverting, for example, regional seismograms (Honda et al. 2004; Koketsu et al. 2004; Nozu and Irikura 2008), teleseismic seismograms (Yamanaka and Kikuchi 2003; Robinson and Cheung 2010), GNSS data (Koketsu et al. 2004; Miyazaki et al. 2004a; Miura et al. 2004), and tsunami data (Tanioka et al. 2004a, b; Romano et al. 2010). There are also source models obtained by inverting two or more different datasets that complement each other. For example, Yagi (2004) jointly inverted teleseismic body waves, which are sensitive to moment release and rupture depth, and regional seismograms, which can constrain the slip process, and they found three different asperities. Koketsu et al. (2004) jointly inverted strong ground motion data and GNSS data and proposed a supershear rupture velocity at the upper part of the fault plane. Romano et al. (2010) conducted joint inversions using the coseismic surface displacements from GNSS and OBP stations and the tsunami waveforms of tide gauges, and they showed main slips occurred 30–80 km northwest of the hypocenter. Recently, Kobayashi et al.

(2021) published two different joint inversion models of the 2003 event using seismic data (teleseismic and strong motion data) including/excluding geodetic data, and both models show ruptures toward the down-dip direction without reaching the Akkeshi-oki region. While coseismic fault slip models of the 2003 Tokachi-oki earthquake are still being published 20 years after the event, there are still no slip models proposed that used tsunami waveforms recorded by the OBPs installed inside the focal region.

Tsunami waveforms have been used in earthquake source studies since the tsunamis are composed of waves caused by seafloor deformation due to fault motion (e.g., Satake 1987, 1989; Satake and Kanamori 1991). In the 1990 s, most tsunami waveforms were recorded at tide gauge stations which are usually located inside bays and harbors, and these tsunami data have strong site effects which mask the signals from the earthquake slip distributions. This could make the estimation of the earthquake source less reliable. However, after the development of OBP observations in the open ocean, tsunami data recorded at the OBPs can record seismic source information without the distortions caused by complex coastal topography (González et al. 1991; Rabinovich and Eblé 2015; Kubota et al. 2020) and greatly have contributed to seismic source studies (e.g., Baba et al. 2005; Satake et al. 2005a; Maeda et al. 2011).

The tsunami analyses have some advantages for retrieving earthquake slip distribution information over seismogram analyses. Firstly, unlike the heterogeneous structural models used for calculating seismic wave propagation, more reliable high-resolution bathymetry data are available for calculating tsunami propagation. This lets us simulate tsunami waveforms more precisely and include not only the leading waves, but also late-arriving dispersive waves (e.g., Saito et al. 2014; Baba et al. 2021) and scattered waves (e.g., Kubota et al. 2018), which significantly contribute to the earthquake source estimation with higher resolution. Secondly, as the tsunami propagation velocity is significantly slower than the earthquake rupture velocity, there is the little trade-off between the slip distribution and the rupture velocity (e.g., Kubota et al. 2018). Therefore, unlike seismic waves whose propagation velocity is comparable to fault rupture velocity, the tsunami waveforms are more useful to constrain slip distribution on the earthquake fault (e.g., Kubota et al. 2018). Even if there are only a few cases, the tsunami signals recorded inside a focal region also have been applied for estimating coseismic slip models (e.g., Kubota et al. 2017, 2022).

When the 2003 Tokachi-oki earthquake occurred, two OBP stations KPG1 and KPG2, located above the source region, clearly recorded the tsunami caused by the earthquake in addition to large dynamic pressure change due to ground motions and significant offset due to the permanent seafloor deformation (e.g., Nosov et al. 2007). Thus, in this study, we carry out inversion analysis to estimate the spatial distribution of fault slips for this event by making use of the OBP tsunami data recorded above the source region as well as from two other OBP stations located approximately 300 km away from the source region. In addition to the tsunami data, we also use GNSS data to obtain better spatial resolution on the deeper portion of the fault plane beneath the onshore area.

Methods

Data

Tsunami data are collected from two OBPs KPG1 and KPG2 installed by JAMSTEC off the southeast coast of Hokkaido (Hirata et al. 2002) and two other OBPs TM1 and TM2 deployed by the Earthquake Research Institute (ERI) of the University of Tokyo off the eastern coast of northeastern Japan (Hino et al. 2001). The stations KPG1 and KPG2 are located at distances of 30 km and 80 km from the epicenter, respectively, and TM1 and TM2 are about 300 km south of the source region. The raw OBP data contain many signals, such as tsunami, seismic waves, ocean acoustic waves, and ocean tides (e.g., Saito and Kubota 2020). To extract tsunami waveforms, we removed tides by subtracting sea-level changes computed from a theoretical tide model which assimilates fully global altimeter data into a hydrodynamic model (Matsumoto et al. 2000) and applied a low-pass filter with a cutoff period of 60 s to remove the effects of seismic motions (Fig. 1b; Tsushima et al. 2012). For the units of tsunami amplitude, we employed a pressure unit of mH_2O which expresses the amount of pressure that is required to lift a 1 m column of water. This unit can be more intuitive for understanding water-depth fluctuations by pressure changes than N/m^2 ($1\ N/m^2 = 0.0001\ mH_2O$). The extracted tsunami waveform from station KPG1 has two peaks with ~0.1 mH_2O between 0 min and 3 min and then the amplitude decreases to ~ −0.4 mH_2O. This offset was brought by the permanent seafloor uplift at KPG1 due to the fault motion. Station KPG2, located further from the epicenter, shows a smaller offset due to the seafloor deformation. At the stations above the source region where the permanent vertical sea-bottom uplift occurs, the ocean-bottom pressure records show offsets when enough time elapses from the earthquake origin time. The stations TM1 and TM2 located far from the source region (~300 km), recorded small peak pressure changes (less than 0.1 mH_2O) as tsunami signals about 30 min later after the earthquake origin time.

Ground deformation caused by the 2003 Tokachi-oki earthquake was recorded onshore by the GNSS Earth

Observation Network System (GEONET), which is operated by the Geospatial Information Authority of Japan (GSI). Larson and Miyazaki (2008) resolved the coseismic static offsets using high-rate GNSS data from 55 stations in Hokkaido and the northern Honshu area. In order to derive accurate static offsets of the Tokachi earthquake, they considered the postseismic deformation following the mainshock and the largest aftershock that occurred about 80 min later. In this study, we use only the horizontal components for the inversions because the vertical component has larger uncertainty than the horizontal components (Larson and Miyazaki 2008).

Fault parameterization

Fault parameter settings are adopted from Tanioka et al. (2004a) in our analysis. The dimension of each subfault is 20 km × 20 km. The fault model of Tanioka et al. (2004a) consists of 6 subfaults along the dip and 8 subfaults along the strike, giving a total number of 48 subfaults, and it is aligned along the plate boundary. The top part of the fault plane does not extend to the trench boundary because the shallower plate boundary was not ruptured by the 2003 Tokachi-oki earthquake (Tanioka et al. 2004b). The fault plane also does not extend under the eastern land portion of Hokkaido; however, some studies have shown that significant slip might have occurred under the land area (e.g., Yagi 2004; Honda et al. 2004; Kobayashi et al. 2021; Romano et al. 2010). To take account of the possibility of slip in the deeper part, we extended the fault plane along the dip direction by adding 8 subfaults along the strike direction (Fig. 1a). Thus, our fault model consists of 7×8 subfaults and the total dimension is 140 km × 160 km along the direction of dip and strike, respectively. For the fault geometries, the strike, dip, and rake of each subfault are set as 230°, 20°, and 109°, respectively, which is the same as Tanioka et al. (2004a).

Joint inversion methodology

We calculated the GNSS static offsets and tsunami waveforms for a unit slip over each subfault. For the GNSS static offsets, we calculated the horizontal components of the instantaneous surface displacements caused by a unit slip over each rectangular subfault assuming a homogeneous elastic half-space (Okada 1985). For the Green's functions of the tsunami waveforms, we calculated seafloor displacements due to a unit slip on each subfault and considered the contribution of the horizontal displacements with the method of Tanioka and Satake (1996). We also assumed that the slip occurred instantaneously (the rise time is zero) and each subfault ruptured simultaneously (the rupture velocity is infinitely large). The total vertical displacements at the seafloor are then used as the initial tsunami height distribution in the tsunami propagation simulations, conducted by solving the linear long-wave equations (e.g., Satake 1995). We set the bathymetry grid interval as 15 arc-sec from GEBCO (GEBCO_2020 Grid), and the simulation region is set in the range of 138°E - 148°E and 32°N - 45°N. The time step of the simulation is 0.5 s, but the sampling period of OBP observations is 1 s, so we decimated the interval of the computed waveforms to 1 s. To invert OBP and GNSS data together, we minimized the following misfit equation:

$$S(\mathbf{m}) = \frac{b}{\mathrm{N}_{\mathrm{OBP}}} \sum \mathbf{w} f_w^2(t) \left(\mathbf{G}_{OBP}\mathbf{m} - \mathbf{O}_{OBP}\right)^2 + \frac{(1-b)}{\mathrm{N}_{\mathrm{GNSS}}} \sum \left(\mathbf{G}_{GNSS}\mathbf{m} - \mathbf{O}_{GNSS}\right)^2 + \alpha^2 \|\mathbf{Sm}\|^2 + \beta^2 \|\mathbf{Im}\|^2. \quad (1)$$

Here, $\mathbf{G}_{OBP}$ and $\mathbf{G}_{GNSS}$ are Green's function matrices of OBP and GNSS data and $\mathbf{O}_{OBP}$ and $\mathbf{O}_{GNSS}$ are vectors of the observed OBP and GNSS data, respectively. $\mathbf{S}$ is a Laplacian operator matrix that controls the model smoothness and $\mathbf{I}$ is the identity matrix. The parameters α and β are weighting values for the smoothing and damping, respectively. In our misfit equation, we also applied different weights to each individual dataset, because the OBP and GNSS data have different physical units and number of data points, so their contributions to the misfit equation need to be balanced. To that end, we introduce a factor b ranging from 0 to 1 to account for the relative influence of one dataset over the other. Since stations farther away have lower amplitudes, we normalize the OBP data using the weighting factor $\mathbf{w}$, applied for each station. This factor is defined as a reciprocal of the maximum amplitude in a signal window. To give more influence to the actual tsunami signal in each OBP waveform, we also multiply the data with a window function $f_w(t)$, defined as

$$f_w(t) = \begin{cases} 0 & \text{if } t \le 0, \\ (1-A)\frac{t}{t_0} + A & \text{if } 0 < t \le t_0, \\ 1 & \text{if } t > t_0, \end{cases} \quad (2)$$

where A is a value of the maximum weight and t_0 is a reference time point. Thus, this function can give more weights for the earlier part of the signal since the origin time. In this study, the maximum weight is set as 2 and the reference time is 30 min. $\mathrm{N}_{\mathrm{OBP}}$ and $\mathrm{N}_{\mathrm{GNSS}}$ are the total number of data points of OBP and GNSS data. To avoid unphysical negative slip, the misfit equation is minimized using the non-negative least-squares method (Lawson and Hanson 1995).

Resolution test

Before we conduct inversions using real observation data of the 2003 Tokachi-oki earthquake, we carried out checkerboard tests in order to test the resolution of each dataset. To design the input model for the test, we used the same fault parameters of our Tokachi-oki earthquake inversion and set the input slip patches as checkers composed of 2 × 2 and 1 × 2 subfaults having a slip of 7 m (Fig. 2a). Synthetic GNSS and OBP data are produced using the input model and the previously calculated Green's function matrices. We added noise for both data. For the synthetic GNSS data, we added Gaussian noise with a standard deviation of 3% of the displacement offset of horizontal components at each station. For the synthetic OBP data, we added similar noise levels as in the real OBP data. We calculated the standard deviation of the observed OBP signal in a 10-min window before the origin time and then used the standard deviation to decide the scale of the Gaussian noise spectrum.

The checkerboard tests clearly show the typical resolving power of each individual dataset (Fig. 2). The GNSS data have a good resolution in the deep portion of the fault plane, while slip patches in the middle and shallow portions are poorly resolved (Fig. 2b). At the shallowest regions, it is difficult to distinguish the outlines of the input slip patches. In contrast, the OBP data are able to sharply resolve the shallow and middle parts of the fault plane, but the resolved slip becomes smoother as depth increases, especially in the extended fault area (Fig. 2c). The joint inversion of synthetic GNSS and OBP data resulted in higher resolution throughout the fault plane compared to the individual dataset inversions due to their complementary nature (Fig. 2d). The joint inversion using both GNSS and OBP data therefore can provide more reliable results across the entire fault plane.

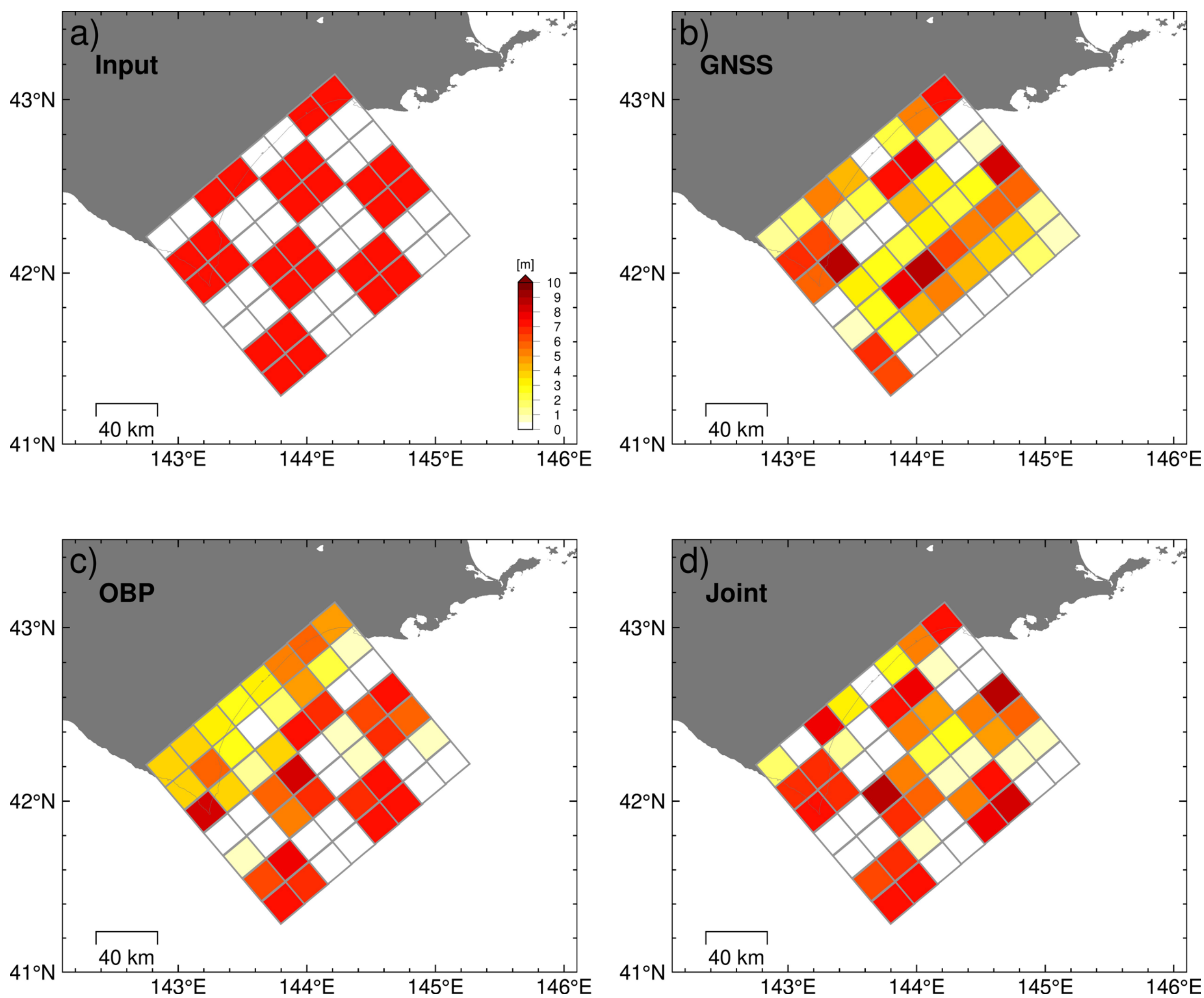

Fig. 2 Checkerboard resolution test results. **a** Checker pattern input model with alternating 0 m and 7 m of slip. The inversion results using **b** GNSS data, **c** OBP data, and **d** both GNSS and OBP data

Results and discussion

Single dataset inversions

Figure 3a shows the slip model inverted using GNSS data. The major slip, which has an amount slip of about 10 m, is located adjacent to the hypocenter and there are also some slips (<3.3 m) in the deepest northwestern portion of the fault. In order to quantify the mismatch between observations and synthetic data, we computed the variance reduction (VR). The VR is defined as $1 - \frac{\sum(O-S)^2}{\sum O^2}$, where O and S are observed and synthetic data, respectively. The VR between observed and synthetic GNSS data is 0.98. We also calculated synthetic OBP waveforms using the slip model obtained by using the GNSS data and then calculated the VR of OBP data (see Additional file 1: Figure S1). The VR was less than 0 indicating that the slip model constructed from GNSS data cannot reproduce the OBP data. This is due to the large slips on the shallower part that generate considerably larger seafloor displacements than those that actually occurred. Unlike the slip model estimated from GNSS data, the inverted slip model using tsunami data of four OBP stations (Fig. 3b) shows that most slips occurred in the deeper portion of the fault plane. The maximum slip is ~ 12 m and is located 70 km away in the down-dip direction from the hypocenter. The VR of OBP and GNSS data using the slip model from OBP data is 0.98 and 0.75, respectively. This model shows more reasonable fitting for both data than the slip model from GNSS data (see Additional file 1: Figure S2). The results of the OBP inversion indicate that the main slip should have occurred in a deeper portion than that of the GNSS inversion.

Joint inversion

We then carried out a joint inversion using both GNSS and OBP observations. For the joint inversions, the data weight b is an important factor in obtaining a reasonable slip model. When the two datasets are given equal weight or when the GNSS data weight is smaller than the OBP weight, we observe significantly smaller synthetic GNSS static offset during the inversions because the relative data norm, which is defined as $\frac{|O_{OBP}|}{|O_{GNSS}|}$, is about 9. This indicates that the magnitude of the OBP data is almost an order of magnitude larger than the GNSS data. Therefore, a much larger GNSS data weight was necessary for the misfit equation to be balanced between OBP and GNSS data. Because the range of the data weight b is between 0 and 1, we attempted to set the value as 0.1. However, this resulted in a model that satisfied the OBP data, but not the GNSS data. We thus adjusted the data weight b to 0.03 which is the point both data are similarly well fit (see Additional file 1: Figure S3a). The smoothing factor α and damping factor β are set as 5×10^{-6} and 0.0012, respectively, and were also determined in a similar way as the factor b (see Additional file 1: Figure S3b).

Our preferred model is shown in Fig. 4a and the fault parameters are listed in Additional file 1: Table S1. The seismic moment is 1.46×10^{21} Nm (M_W 8.1), assuming a rigidity of 40 GPa. In general, the slips from our joint

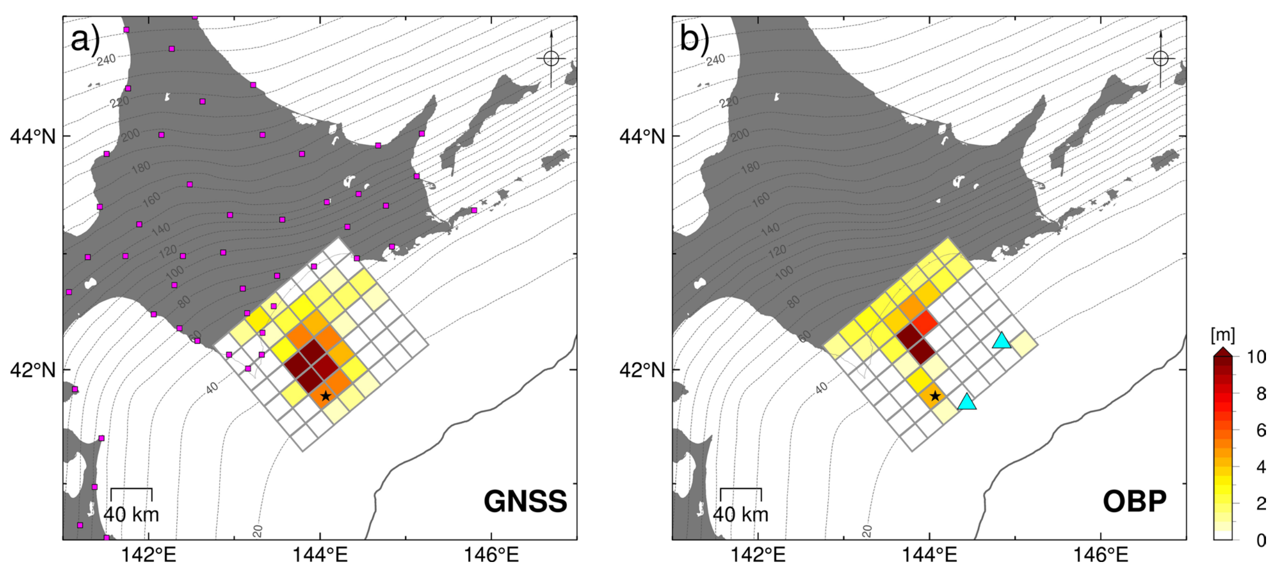

Fig. 3 Slip distribution models of the 2003 Tokachi-oki earthquake from single dataset inversions using **a** GNSS static offsets only and **b** tsunami waveforms of OBPs only. The black star indicates the epicenter of the Tokachi earthquake. Magenta squares indicate GNSS stations and cyan triangles are OBPs. Gray dashed lines indicate the plate-boundary depth (Koketsu et al. 2012) with a 10-km contour interval and the gray solid line is the trench axis

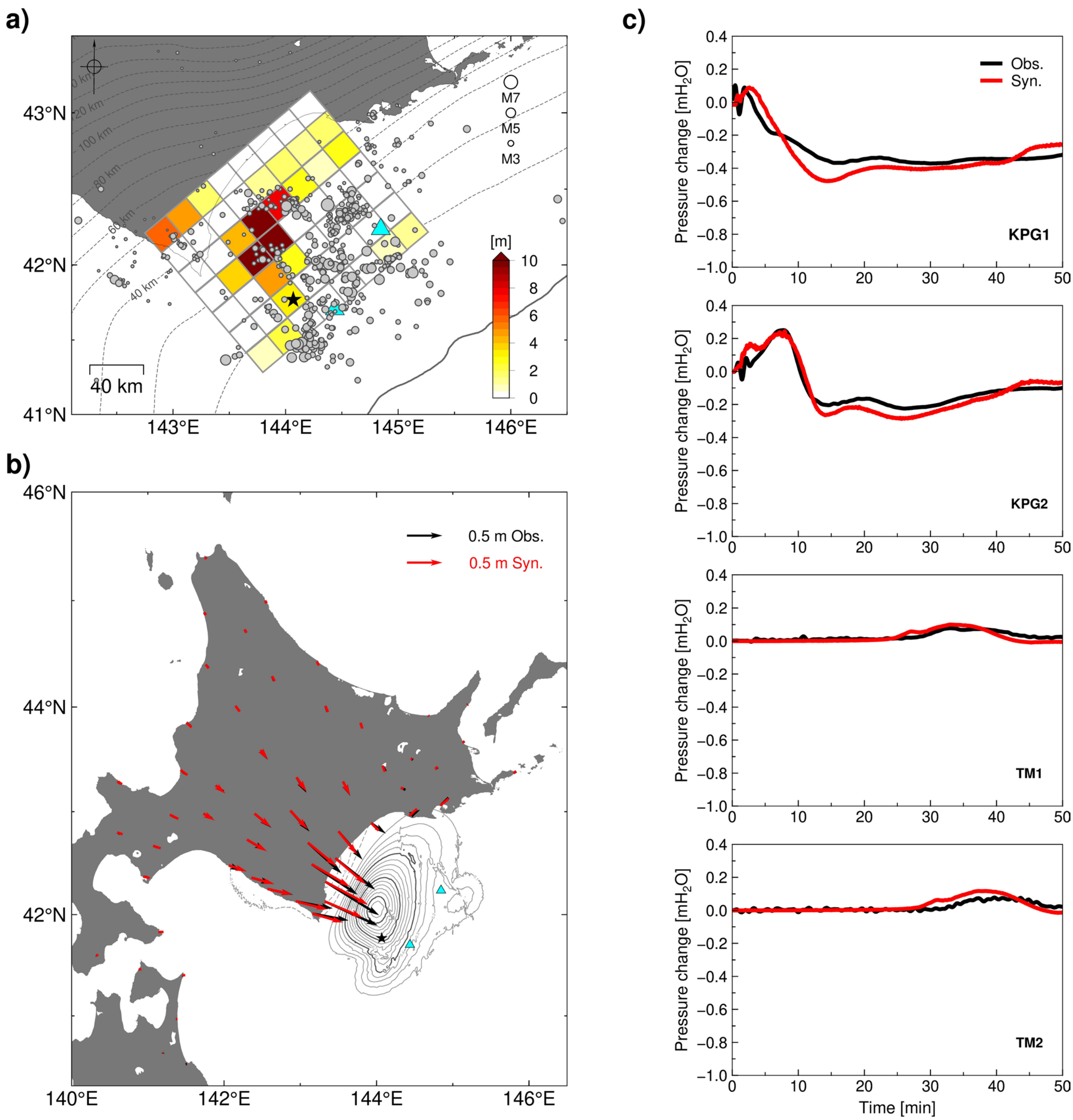

Fig. 4 Joint inversion results. **a** The slip distribution model obtained by the joint inversion of GNSS and OBP data. The gray circles indicate aftershocks (catalog of ISC and JMA) occurring within one week after the mainshock. **b** Comparison of GNSS static offsets between observations (black color) and synthetic results (red color). The gray contours indicate the total vertical displacement computed using the joint inversion result. The light gray line and the dark gray line represent 0.1 m and 0.5 m intervals, respectively. **c** Comparisons of tsunami waveforms between observations (black) and synthetic results (red) at four OBPs

inversion are spatially concentrated in the down-dip area from the hypocenter and there are almost no slips on the southeastern portion of the fault plane. The main slip patch with an amount of slip of ~15 m is located approximately 40 km northwest of the hypocenter. This is located between the major slip regions resulting from each single dataset inversion, and the maximum slip of the joint inversion is larger than the maximum slips of the individual dataset inversions. Another slip patch (~6 m) is at the western edge in the deepest portion (50–60 km) of the fault plane, which is a new feature appearing only in the joint inversion results. In the deeper part (>40 km), aseismic slip due to the frictional properties at higher temperatures can be expected rather than coseismic rupture. To investigate whether it is a true feature of the 2003 Tokachi-oki earthquake or an artifact of the inversion, we conducted additional analyses and discussed the slip at the edge in the section "Interseismic slip deficit and coseismic slip distributions".

The synthetic data obtained by using the preferred model generally show good agreement with the observations. The calculated horizontal components at the 55 GNSS stations agree well with observations, except for smaller offsets at the stations close to the source (Fig. 4b). Figure 4c shows comparisons between OBP observations and computed tsunami waveforms. They also show reasonable agreement with the observed data. The VR values of GNSS data only, OBP data only, and joint data are 0.95, 0.93, and 0.95, respectively, and these values show that the slip model from the joint inversion was able to fit both datasets simultaneously to a satisfactory degree. However, the results of the joint inversion also show that neither the GNSS station record nor the submarine tsunami record (KPG1) is perfectly reproduced close to the fault's major slip. On the other hand, the inversion using only GNSS or OBP records (Additional file 1: Figures S1 and S2) reproduces each data better. One reason may be that assumptions such as all subfaults having the same fault geometry in the inversion analysis are too simple to reproduce the actual data. To obtain better results, we can consider 3-D subsurface structure or non-planar fault geometry, which can be a topic for future study.

Comparison with tide gauge data

To verify whether our estimated slip model would accurately reproduce the tsunami generated after the 2003 Tokachi-oki earthquake, we performed a tsunami simulation using our preferred model from the joint inversion and compared it with tsunami observations not used for the inversion. For the comparison, we first collected tsunami observations from tide gauges located in Hokkaido and northern Honshu (Fig. 1) by digitizing tide records from Nagai and Ogawa (2004). The digitized tidal records are resampled to 1 Hz and smoothed by applying a moving average filter with a time window of 60 s. We then carried out the tsunami simulation by solving the nonlinear long-wave equation (e.g., Satake 1995; Saito et al. 2014) to include nonlinear effects near the coasts. Comparisons between observed and synthetic tsunami waveforms are shown in Fig. 5. On the whole, the resulting simulated waveforms show excellent agreement with the observations. The first peak arrivals of the synthetic waveforms are slightly earlier than the observations, but the differences are negligible at some stations such as Hachinohe, TomakomaiW, and Mutuogawara. At stations located near the source such as Hanasaki, Akkeshi, Kushiro, and Tokachioki, the amplitudes and arrival times of simulated tsunamis match well with the observed tsunami data. At Hachinohe, Mutsuogawara, and Kuji stations located on the eastern coast of northern Honshu, the first phases of simulated waves have two blunt peaks and smaller amplitudes than the observations. Although we did not use tide gauge tsunami data in the inversion, simulated tsunami waveforms using the estimated slip model fit very well with tide gauge records. This supports the validity of the estimated slip model.

Effects of tsunamis inside the focal area on slip estimations

Unlike previous studies of estimating slips for the 2003 Tokachi-oki earthquake, this study utilized the OBP data inside the focal regions. In order to investigate how well slip models derived without using the OBP data can reproduce tsunami waveforms in the focal region, we compared tsunami observations recorded at OBP stations KPG1 and KPG2 and tsunami waveforms synthesized using the source models of Tanioka et al. (2004a), Romano et al. (2010), and Kobayashi et al. (2021). The slip model of Tanioka et al. (2004a) (Fig. 6a) has a similar slip distribution pattern as our model except for the maximum slip (~4 m) is a lot smaller than our slip model. At station KPG1, the computed tsunami waveforms show smaller amplitudes compared to the observations (Fig. 6d). Moreover, the model could not reproduce the largest peak at the KPG2 (Fig. 6g). In the case of Romano et al. (2010) model, which is obtained from a joint inversion of GNSS data and tsunami data from tide gauges (Fig. 6b), the tsunami peaks are missing around 3 min and 7 min at KPG1 and KPG2, respectively (Fig. 6e, h). The model of Kobayashi et al. (2021) is obtained by using teleseismic and regional seismograms and GNSS data (Fig. 6c). This model resulted in too much offset at KPG1 and a larger rise at KPG2 compared to the observations (Fig. 6f, i). This indicates that their fault model caused a larger seafloor deformation near station KPG1 than the actual fault motion could have caused. The fault plane of Kobayashi et al. (2021) extends to northeastern Hokkaido and the trench axis. The slips on the southeastern fault plane generate substantial seafloor deformation along the trench axis, and this could be recorded as a large amplitude peak at KPG2. The synthetic tsunami waveforms calculated using the three source models show considerable differences with the OBP observations, even though the models had a good agreement with the data used for their inversions, such as seismograms, GNSS data, and tide gauge tsunami records. These comparisons suggest that tsunami waveforms recorded in the focal region can

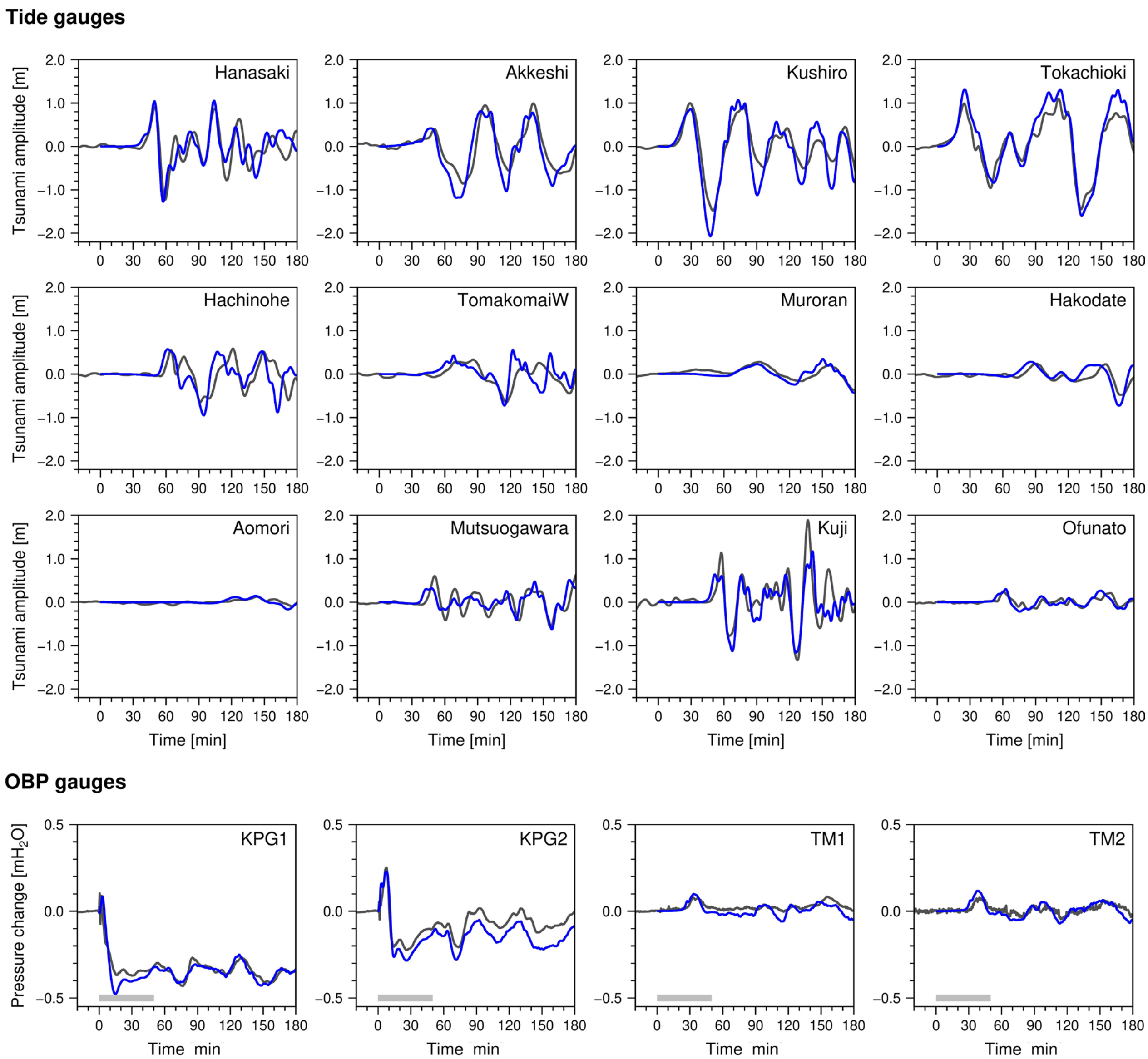

Fig. 5 Tsunami waveform comparison between observations of tide and OBP stations (dark gray line) and simulation results (blue line). The thick gray line on the time axes of OBP graphs indicates a data length used for the inversions

provide critical information that constrains the magnitude and spatial distribution of fault slips.

Interseismic slip deficit and coseismic slip distributions

Several postseismic slip studies of the 2003 Tokachi earthquake have been conducted (Miyazaki et al. 2004b; Ozawa et al. 2004; Baba et al. 2006; Itoh et al. 2019), and the main coseismic slip areas estimated in this study mostly avoid the regions where the postseismic slips occurred, suggesting that the region in which the stress is accumulated for the 2003 earthquake may be surrounded by aseismic slip zones where no stress is accumulated as Baba et al. (2006). Moreover, the aftershocks ($M \geq 1.0$) that occurred in the following week after the mainshock were active in regions where little coseismic slip occurred (Fig. 4a). The coseismic slips by the 2003 event released the slip deficit generated in and around the locked areas on the plate boundary during the interseismic period. Hashimoto et al. (2009) analyzed GNSS data between 1996 and 2000 to obtain the rate of the slip deficit during the interseismic period. Their results show a distinct area with a size of ~6400 km^2 with a slip-deficit rate larger than 6 cm/yr in and around the main coseismic slip area. Also, Fukuyama et al. (2009) conducted a dynamic

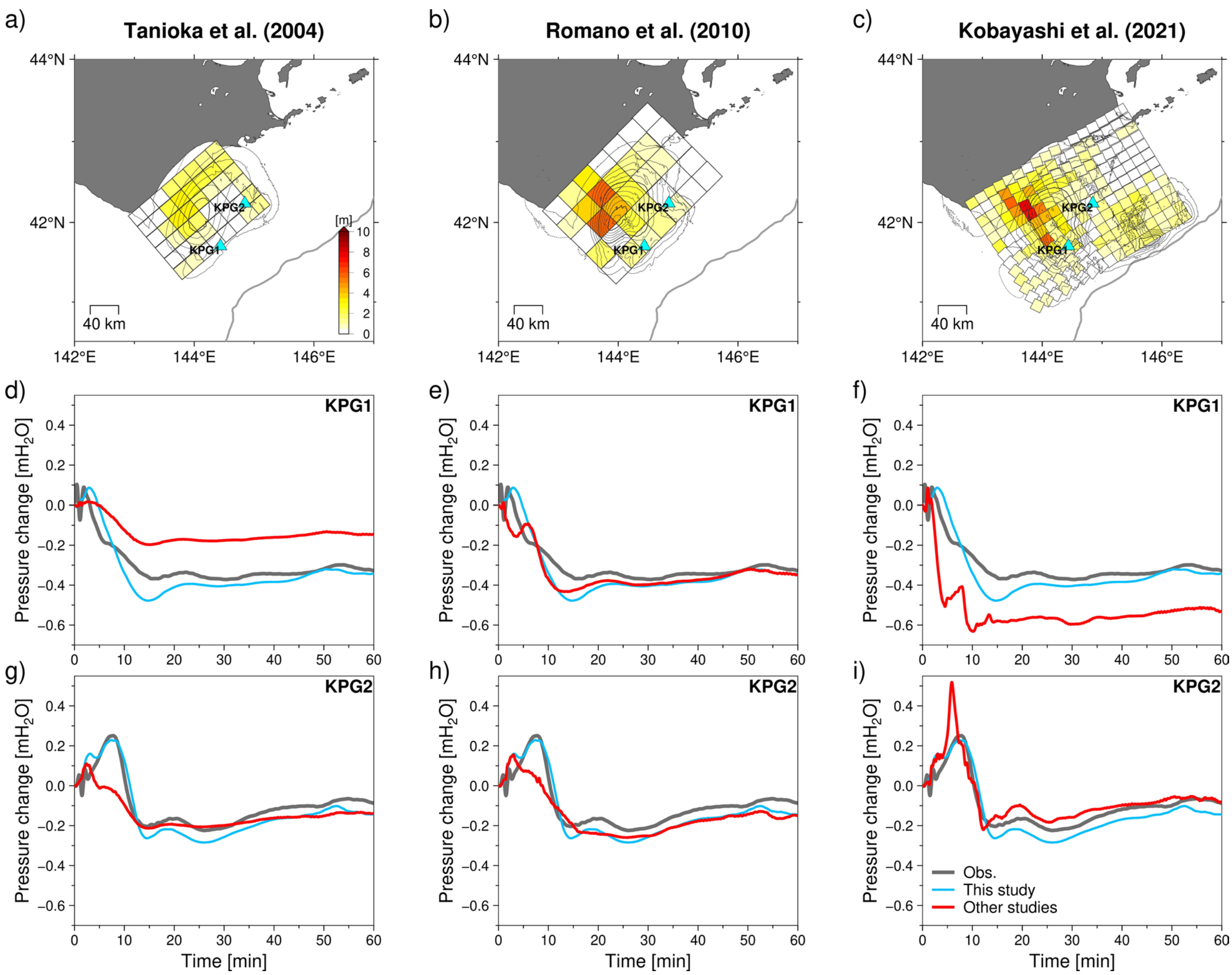

Fig. 6 Comparison with other source models. **a**-**c** Source models of the 2003 Tokachi-oki earthquake published by Tanioka et al. (2004a), Romano et al. (2010), Kobayashi et al. (2021). The contour lines are the total vertical displacement with 0.1 m (light gray) and 0.5 m (dark gray) intervals. **d**-**i** Comparison between the observed tsunamis at OBP stations KPG2 and KPG2 (gray), simulated tsunami waveforms using the three source models (red), and simulated waveforms using our model (light blue)

rupture simulation for the coseismic slip of the 2003 Tokachi-oki earthquake, taking into account the stress accumulation process detected by the GNSS analysis. If the slip deficit has been accumulated with a constant deficit rate since the last great earthquake in 1952 (e.g., Hirata et al. 2003; Satake et al. 2006), the area should accumulate about 3 m of slip deficit on average. The seismic moment corresponding to this slip deficit is about 7.68×10^{20} Nm, while the main slip area of the 2003 earthquake is 9.92×10^{20} Nm. The seismic moment based on the slip deficit is almost the same but slightly smaller. Due to our assumptions in estimating the expected magnitude from the slip deficit, it is not surprising that this expected magnitude is different from the actual magnitude. First, as only onshore GNSS data were available, we might have failed to detect some of the offshore slip deficit distributions. Second, although we assume that the stress has been accumulated from 1952 to 2003, i.e., the stress was completely released at the 1952 event, we cannot rule out the possibility that stress was not completely released during the 1952 event with some stress remaining. Third, we assume that the slip-deficit rate has been constant since 1952, but this is not always true. The deficit rate can change in time (Ozawa et al. 2007) and it can also turn to negative (Nishimura et al. 2004), which means that some zones on the plate boundary can slip over the convergence rate.

The secondary slip patch (~6 m), which is at the deep (50–60 km) western edge of the fault plane, is a new feature that appears in the joint inversion. While several previous studies also showed notable slips in the deep portion of their fault models (e.g.,Koketsu et al. 2004; Yagi 2004; Honda et al. 2004; Robinson and Cheung 2010), the amount of slip in those depths is difficult to understand because aseismic slips due to the frictional properties at higher temperature are expected in the deeper part (>40 km) under the Earth's surface rather than coseismic ruptures. To identify whether the slips at the corner of the fault plane are a true feature of the 2003 Tokachi-oki earthquake or an inversion artifact, we conducted additional joint inversion analysis applying two more different fault dimensions consisting of 6 × 8 subfaults and 9 × 10 subfaults. The 6 × 8 model is the same dimension as Tanioka et al. (2004a) used for their inversion and the 9 × 10 model is extended deeper along the dip direction and also in the southwestern direction. The two models yield the dominant slips in almost similar locations in the down-dip area from the hypocenter as our slip model, which is composed of 7 × 8 subfaults, but the deep slip patch changes depending on the subfault settings (Fig. 7). The two 6 × 8 and 9 × 10 models resulted in the VR of 0.94 and 0.95, respectively, which are almost the same as our estimated slip model (0.95). The areas outside of the dominant slip region showed different slip distributions according to the subfault parameterization, but these brought no significant differences in the synthetic GNSS and OBP data (Fig. 7d and e). Based on the results of inversions, the deep slip at the corner of the fault plane of our joint model (7 × 8 subfaults) can be artificial. In order to estimate how the deep slip patch contributes to the calculated records, we calculated the VR of the GNSS and OBP data after forcing the amount of slip to zero. The VR of GNSS and OBP are 0.93 and 0.94, respectively. Compared to the original slip model, the VR of the GNSS data slightly decreased, whereas the VR of the OBP data is the same. Since the secondary slip patch is beneath southern Hokkaido, there is almost no effect on tsunami amplitude, whereas synthesized GNSS data were slightly changed (see Additional file 1: Figure S4). The complicated subsurface structure of southern Hokkaido would generate differences between the observed and synthetic GNSS records, and the difference would contribute to the generation of artificial slips at the edge of the fault plane. In future study, it is important to investigate how realistic complicated structures such as 3-D subsurface structures and non-planar fault geometry affect the results of the inversion analyses. The results of this study will work as a good reference for further development.

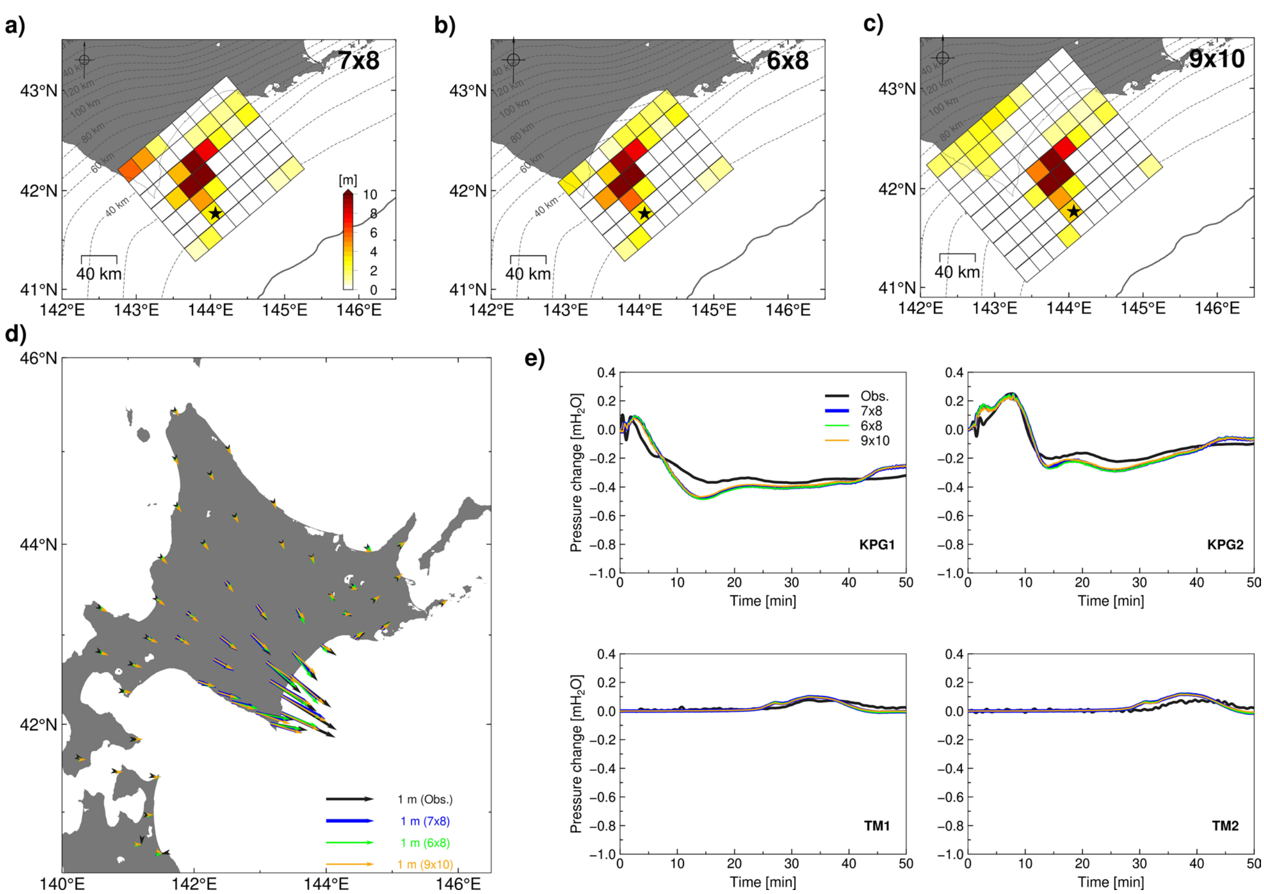

Fig. 7 Results of the joint inversions applying different fault dimensions. Inversion results for **a** 7 × 8, **b** 6 × 8, **c** 9 × 10 subfaults settings. **d** Comparisons of observed and synthesized GNSS data. **e** Comparisons of observed and synthesized OBP data

Conclusions

The spatial distribution of fault slips for the 2003 Tokachi-oki earthquake was estimated by inverting OBP tsunami records and GNSS data simultaneously. For the inversion of this event, tsunami data from OBP stations located almost directly above the focal region was utilized for the first time. The estimated slip model from the joint inversion has a dominant slip patch located 40 km south of the epicenter with a large amount of peak slip (~ 15 m) within the concentrated domain. This slip pattern supports the idea that the 2003 Tokachi-oki earthquake released the slip deficit accumulated by the locked area embedded in stable slip regions on the southernmost Kuril subduction zone. Moreover, this study also confirms that tsunami observations inside focal areas can provide excellent constraints for the amount and location of slip on the fault plane.

Abbreviations

ERI	Earthquake Research Institute, the University of Tokyo
GEBCO	General Bathymetric Chart of the Oceans
GEONET	GNSS Earth Observation Network System
GNSS	Global Navigation Satellite System
GSI	Geospatial Information Authority of Japan
ISC	International Seismological Centre
JAMSTEC	Japan Agency for Marine-Earth Science and Technology
JMA	Japan Meteorological Agency
OBPs	Ocean-Bottom Pressure gauges
OBS	Ocean-Bottom Seismometer
SNR	Signal-to-Noise Ratio
VR	Variance Reduction

Supplementary Information

The online version contains supplementary material available at https://doi.org/10.1186/s40623-023-01864-x.

Additional file 1: Table S1. Subfault parameters of slip model. **Figure S1.** a) The slip distribution model using GNSS data. b) Comparison of GNSS static offsets between observations (black color) and inverted GNSS static offset (red color). c) Comparisons of tsunami observations (black color) and calculated tsunami waveforms (red color). **Figure S2.** a) The slip distribution model using OBP data. b) Comparison of GNSS static offsets between observations (black color) and calculated GNSS static offset (red color). c) Comparisons of tsunami observations (black color) and inverted tsunami waveforms (red color). **Figure S3.** a) Variance reduction of the GNSS and OBP data depending on the data weight factor b in the joint inversions. The blue line in the inset box indicates the value of b that the VR of the two data crosses and the red line is the value that we applied in our joint inversion. b) Variance reduction of the GNSS and OBP data depending on the moothing factor α and damping factor β. Among the smoothing factors, 5×10^{-6} resulted in the best VR for both data. When 5×10^{-6} is applied for smoothing factor, the VR of the two data crosses at the damping factor 0.002 (blue line). The VR of OBP is almost stable after the cross point, while the VR of GNSS data is increasing. Therefore, a slightly smaller value of 0.0012 (red line) is applied for the damping factor in this study. Triangle and circle symbols indicate the GNSS and OBP data, respectively, and colors indicate the smoothing factors. **Figure S4.** a) The slip distribution model after removing slips of the second slip patch at the corner of the fault plane (green box). b) Comparison of GNSS static offsets between observations (gray color), inverted results using the slip model from joint inversion (blue color), and synthetic GNSS data using the revised model after removing the second slip patch from the joint inversion model (green color). c) Comparisons of tsunami waveforms.

Acknowledgements

We would like to thank the editor and reviewers for taking the time to review our manuscript and we appreciate all the constructive comments and suggestions which helped us to improve the manuscript. A number of figures were produced using the Generic Mapping Tools version 6 (Wessel et al. 2019). The Python-based package SciPy (Virtanen et al. 2020) is used for inversion.

Author contributions

SK analyzed data and wrote the manuscript. TS contributed to the design of the study and gave instructions for the methods and analyses. TK prepared and processed tsunami data of OBP and tide gauges. SC supervised this work. SK, TS, TK, and SC interpreted the data and discussed the results. All authors read and approved the final manuscript.

Funding

This study was supported by the Korea Meteorological Administration Research and Development Program under Grant KMI 2022-00810, by the National Research Foundation of Korea (NRF) grant funded by the Korean government (MSIT) (2019R1A2C208506111), by Basic Science Research Program through the NRF funded by the Ministry of Education (No. 2019R1A6A1A03033167).

Availability of data and materials

Subfault parameters of the 2003 Tokachi-oki earthquake inverted by the joint inversion are shown in Additional file 1: Table S1. OBP data of KPG1 and KPG2 were provided by JAMSTEC (Hirata et al. 2002) and OBP data of TM1 and TM2 were provided by ERI (Hino et al. 2001), upon reasonable requests to them. The static offset data of the GEONET stations were processed by Larson and Miyazaki (2008) and collected from https://doi.org/10.1186/BF03352831. The aftershock list of the 2003 Tokachi-oki earthquake can be downloaded at https://ds.iris.edu/wilber3/find_event. The bathymetry data provided by GEBCO is available at https://www.gebco.net/data_and_products/historical_data_sets#gebco_2020. The source model by Tanioka et al. (2004a) is collected from Table 1 in https://doi.org/10.4294/zisin1948.57.2_75. The source model by Romano et al. (2010) is available from supporting information files in https://doi.org/10.1029/2009JB006665. The source model by Kobayashi et al. (2021) is available at the finite-fault source model database http://equake-rc.info/srcmod/. The program of NAO.99b tidal prediction system which is developed by Matsumoto et al. (2000) is available at https://www.miz.nao.ac.jp/staffs/nao99/index_En.html. Surface deformation calculation program by Okada (1985) is able to download in https://www.bosai.go.jp/e/dc3d.html.

Declarations

Competing interests

The authors declare that they have no competing interests.

Author details

[1]Department of Earth and Environmental Sciences, Korea University, 145 Anam-ro, Seongbuk-gu, Seoul 02841, South Korea. [2]National Research Institute for Earth Science and Disaster Resilience, 3-1 Tennodai, Tsukuba, Ibaraki 305-0006, Japan. [3]Department of Geophysics, Kangwon National University, 1 Gangwondaehakgil, Chuncheon, Gangwon-do 24341, South Korea.

Received: 23 December 2022 Accepted: 29 June 2023
Published online: 18 July 2023

References

Baba T, Cummins PR, Hori T (2005) Compound fault rupture during the 2004 off the Kii Peninsula earthquake (*M* 7.4) inferred from highly resolved coseismic sea-surface deformation. Earth Planets Space 57:167–172. https://doi.org/10.1186/BF03351810

Baba T, Hirata K, Hori T, Sakaguchi H (2006) Offshore geodetic data conducive to the estimation of the afterslip distribution following the 2003 Tokachi-oki earthquake. Earth Planet Sci Lett 241:281–292. https://doi.org/10.1016/j.epsl.2005.10.019
Baba T, Chikasada N, Imai K, Tanioka Y, Kodaira S (2021) Frequency dispersion amplifies tsunamis caused by outer-rise normal faults. Sci Rep 11:20064. https://doi.org/10.1038/s41598-021-99536-x
Fukuyama E, Ando R, Hashimoto C, Aoi S, Matsu'ura M (2009) A physics-based simulation of the 2003 Tokachi-oki, Japan, earthquake to predict strong ground motions. Bull Seismol Soc Am 99(6):3150–3171. https://doi.org/10.1785/0120080040
González FI, Mader CL, Eble MC, Bernard EN (1991) The 1987–88 Alaskan Bight tsunamis: Deep ocean data and model comparisons. In: Bernard EN (ed) Tsunami Hazard. Springer, Berlin, pp 119–139. https://doi.org/10.1785/0120080040
Hashimoto C, Noda A, Sagiya T, Matsu'ura M (2009) Interplate seismogenic zones along the Kuril-Japan trench inferred from GPS data inversion. Nat Geosci 2:141–144. https://doi.org/10.1038/ngeo421
Hino R, Tanioka Y, Kanazawa T, Sakai S, Nishino M, Suyehiro K (2001) Micro-tsunami from a local interplate earthquake detected by cabled offshore tsunami observation in northeastern Japan. Geophys Res Lett 28(18):3533–3536. https://doi.org/10.1029/2001GL013297
Hirata K, Aoyagi M, Mikada H, Kawaguchi K, Kaiho Y, Iwase R, Morita S, Fujisawa I, Sugioka H, Mitsuzawa K, Suyehiro K, Kinoshita H, Fujiwara N (2002) Real-time geophysical measurements on the deep seafloor using submarine cable in the southern Kurile subduction zone. IEEE J Ocean 27(2):170–181. https://doi.org/10.1109/JOE.2002.1002471
Hirata K, Geist E, Satake K, Tanioka Y, Yamaki S (2003) Slip distribution of the 1952 Tokachi-Oki earthquake (*M* 8.1) along the Kuril trench deduced from tsunami waveform inversion. J Geophys Res Solid Earth 108(B4):2196. https://doi.org/10.1029/2002JB001976
Hirata K, Tanioka Y, Satake K, Yamaki S, Geist EL (2004) The tsunami source area of the 2003 Tokachi-oki earthquake estimated from tsunami travel times and its relationship to the 1952 Tokachi-oki earthquake. Earth Planets Space 56:367–372. https://doi.org/10.1186/BF03353066
Hirata K, Satake K, Yamaki S, Tanioka Y, Yamanaka Y, Nishimura T (2007) Examination of northeast edge of the 1952 Tokachi-oki earthquake tsunami source based on eyewitness accounts stated in previously published reports (in Japanese with English abstract). Zisin 60(1):21–41. https://doi.org/10.4294/zisin.60.21
Honda R, Aoi S, Morikawa N, Sekiguchi H, Kunugi T, Fujiwara H (2004) Ground motion and rupture process of the 2003 Tokachi-oki earthquake obtained from strong motion data of K-NET and KiK-net. Earth Planets Space 56:317–322. https://doi.org/10.1186/BF03353058
Ichiyanagi M, Takahashi H, Motoya Y, Kasahara M, Mikada H, Hirata K, Suyehiro K (2003) An unusual seismic activity from October, 2001 to June, 2002, off Tokachi, Hokkaido, Japan (in Japanese with English abstract). Geophys Bull Hokkaido Univ 66:87–99. https://doi.org/10.14943/gbhu.66.87
Itoh Y, Nishimura T, Ariyoshi K, Matsumoto H (2019) Interplate slip following the 2003 Tokachi-oki earthquake from ocean bottom pressure gauge and land GNSS data. J Geophys Res Solid Earth 124:4205–4230. https://doi.org/10.1029/2018JB016328
Kobayashi H, Koketsu K, Miyake H, Kanamori H (2021) Similarities and differences in the rupture processes of the 1952 and 2003 Tokachi-oki earthquakes. J Geophys Res Solid Earth 126:e2020JB020585. https://doi.org/10.1029/2020JB020585
Koketsu K, Hikima K, Miyazaki S, Ide S (2004) Joint inversion of strong motion and geodetic data for the source process of the 2003 Tokachi-oki, Hokkaido, earthquake. Earth Planets Space 56:329–334. https://doi.org/10.1186/BF03353060
Koketsu K, Miyake H, Suzuki H (2012) Japan integrated velocity structure model version 1. In: Proceedings of the 15th World Conference on Earthquake Engineering, Lisbon, 24-28 September 2012. https://www.iitk.ac.in/nicee/wcee/article/WCEE2012_1773.pdf. Accessed 15 Jun 2023
Kubota T, Hino R, Inazu D, Ito Y, Iinuma T, Ohta Y, Suzuki S, Suzuki K (2017) Coseismic slip model of offshore moderate interplate earthquakes on March 9, 2011 in Tohoku using tsunami waveforms. Earth Planet Sci Lett 458:241–251. https://doi.org/10.1016/j.epsl.2016.10.047
Kubota T, Saito T, Ito Y, Kaneko Y, Wallace LM, Suzuki S, Hino R, Henrys S (2018) Using tsunami waves reflected at the coast to improve offshore earthquake source parameters: Application to the 2016 Mw 7.1 Te Araroa earthquake, New Zealand. J Geophys Res Solid Earth 123:8767–8779. https://doi.org/10.1029/2018JB015832
Kubota T, Saito T, Chikasada N, Suzuki W (2020) Ultrabroadband seismic and tsunami wave observation of high-sampling ocean-bottom pressure gauge covering periods from seconds to hours. Earth Space Sci 7:e2020EA001197. https://doi.org/10.1029/2020EA001197
Kubota T, Saito T, Hino R (2022) A new mechanical perspective on a shallow megathrust near-trench slip from the high-resolution fault model of the 2011 Tohoku-Oki earthquake. Prog Earth Planet Sci 9:68. https://doi.org/10.1186/s40645-022-00524-0
Larson KM, Miyazaki S (2008) Resolving static offsets from high-rate GPS data: the 2003 Tokachi-oki earthquake. Earth Planets Space 60:801–808. https://doi.org/10.1186/BF03352831
Lawson CL, Hanson RJ (1995) Solving least squares problems. SIAM Phila PA. https://doi.org/10.1137/1.9781611971217
Maeda T, Furumura T, Sakai S, Shinohara M (2011) Significant tsunami observed at ocean-bottom pressure gauges during the 2011 off the Pacific coast of Tohoku earthquake. Earth Planets Space 63:803–808. https://doi.org/10.5047/eps.2011.06.005
Matsumoto K, Takanezawa T, Ooe M (2000) Ocean tide models developed by assimilating TOPEX/POSEIDON altimeter data into hydrodynamical model: a global model and a regional model around Japan. J Oceanogr 56:567–581. https://doi.org/10.1023/A:1011157212596
Miura S, Suwa Y, Hasegawa A, Nishimura T (2004) The 2003 M8.0 Tokachi-Oki earthquake - how much has the great event paid back slip debts? Geophys Res Lett 31:L05613. https://doi.org/10.1029/2003GL019021
Miyazaki S, Larson KM, Choi K, Hikima K, Koketsu K, Bodin P, Haase J, Emore G, Yamagiwa A (2004a) Modeling the rupture process of the 2003 September 25 Tokachi-Oki (Hokkaido) earthquake using 1-Hz GPS data. Geophys Res Lett 31:L21603. https://doi.org/10.1029/2004GL021457
Miyazaki S, Segall P, Fukuda J, Kato T (2004b) Space time distribution of afterslip following the 2003 Tokachi-oki earthquake: Implications for variations in fault zone frictional properties. Geophys Res Lett 31:L06623. https://doi.org/10.1029/2003GL019410
Motoya Y (1999) Clustered seismic activity in and around Hokkaido (in Japanese with english abstract). Geophys Bull Hokkaido Univ 62:15–24. https://doi.org/10.14943/gbhu.62.15
Nagai T, Ogawa H (2004) Characteristic of the 2003 Tokachi-off earthquake tsunami profile. Technical note of the port airport research institute. https://pari-y8sv.movabletype.biz/en/2004/03/200403107001.html. Accessed 15 Jun 2023
Nanayama F, Satake K, Furukawa R, Shimokawa K, Atwater BF, Shigeno K, Yamaki S (2003) Unusually large earthquakes inferred from tsunami deposits along the Kuril trench. Nature 424:660–663. https://doi.org/10.1038/nature01864
Nanayama F, Furukawa R, Shigeno K, Makino A, Soeda Y, Igarashi Y (2007) Nine unusually large tsunami deposits from the past 4000 years at Kiritappu marsh along the southern Kuril trench. Sediment Geol 200(3–4):275–294. https://doi.org/10.1016/j.sedgeo.2007.01.008
Nishimura T, Hirasawa T, Miyazaki S, Sagiya T, Tada T, Miura S, Tanaka K (2004) Temporal change of interplate coupling in northeastern Japan during 1995–2002 estimated from continuous GPS observations. Geophys J Int 157:901–916. https://doi.org/10.1111/j.1365-246X.2004.02159.x
Nosov MA, Kolesov SV, Denisova AV, Alekseev AB, Levin BV (2007) On the near-bottom pressure variations in the region of the 2003 Tokachi-Oki tsunami source. Oceanology 47:26–32. https://doi.org/10.1134/S0001437007010055
Nozu A, Irikura K (2008) Strong-motion generation areas of a great subduction-zone earthquake: waveform inversion with empirical Green's functions for the 2003 Tokachi-oki earthquake. Bull Seismol Soc Am 98(1):180–197. https://doi.org/10.1785/0120060183
Okada Y (1985) Surface deformation due to shear and tensile faults in a half-space. Bull Seismol Soc Am 75(4):1135–1154. https://doi.org/10.1785/BSSA0750041135
Ozawa S, Kaidzu M, Murakami M, Imakiire T, Hatanaka Y (2004) Coseismic and postseismic crustal deformation after the M_w 8 Tokachi-oki earthquake in Japan. Earth Planets Space 56:675–680. https://doi.org/10.1186/BF03352530
Ozawa S, Suito H, Nishimura T, Tobita M, Munekane H (2007) Possibility of recovery of slip deficit rate between the North American plate and the

Pacific plate off Sanriku, northeast Japan. Geophys Res Lett 34:L20308. https://doi.org/10.1029/2007GL030477
Rabinovich AB, Eblé MC (2015) Deep-ocean measurements of tsunami waves. Pure Appl Geophys 172:3281–3312. https://doi.org/10.1007/s00024-015-1058-1
Robinson D, Cheung L (2010) Source process of the M_w 8.3, 2003 Tokachi-Oki, Japan earthquake and its aftershocks. Geophys J Int 181:334–342. https://doi.org/10.1111/j.1365-246X.2010.04513.x
Romano F, Piatanesi A, Lorito S, Hirata K (2010) Slip distribution of the 2003 Tokachi-oki M_w 8.1 earthquake from joint inversion of tsunami waveforms and geodetic data. J Geophys Res Solid Earth 115:B11313. https://doi.org/10.1029/2009JB006665
Saito T, Kubota T (2020) Tsunami modeling for the deep sea and inside focal areas. Annu Rev Earth Planet Sci 48:121–145. https://doi.org/10.1146/annurev-earth-071719-054845
Saito T, Inazu D, Miyoshi T, Hino R (2014) Dispersion and nonlinear effects in the 2011 Tohoku-Oki earthquake tsunami. J Geophys Res Oceans 119:5160–5180. https://doi.org/10.1002/2014JC009971
Satake K (1987) Inversion of tsunami waveforms for the estimation of a fault heterogeneity: Method and numerical experiments. J Earth Space Phys 35:241–254. https://doi.org/10.4294/jpe1952.35.241
Satake K (1989) Inversion of tsunami waveforms for the estimation of heterogeneous fault motion of large submarine earthquakes: The 1968 Tokachi-oki and 1983 Japan Sea earthquakes. J Geophys Res Solid Earth 94(B5):5627–5636. https://doi.org/10.1029/JB094iB05p05627
Satake K (1995) Linear and nonlinear computations of the 1992 Nicaragua earthquake tsunami. Pure Appl Geophys 144:455–470. https://doi.org/10.1007/BF00874378
Satake K (2017) Great earthquakes in the 17th century along the Kuril and Japan Trenches (in Japanese with English abstract). Bull Earthq Res Inst Univ Tokyo 92:31–47. https://doi.org/10.15083/0000051809
Satake K, Kanamori H (1991) Use of tsunami waveforms for earthquake source study. Nat Hazards 4:193–208. https://doi.org/10.1007/BF00162787
Satake K, Baba T, Hirata K, Iwasaki SI, Kato T, Koshimura S, Takenaka J, Terada Y (2005) Tsunami source of the 2004 off the Kii Peninsula earthquakes inferred from offshore tsunami and coastal tide gauges. Earth Planets Space 57:173–178. https://doi.org/10.1186/BF03351811
Satake K, Nanayama F, Yamaki S, Tanioka Y, Hirata K (2005b) Variability among tsunami sources in the 17th–21st centuries along the soutehrn Kuril Trench. In: Satake K (ed) Tsunamis, vol 23. Springer, Dordrecht, pp 157–170, https://doi.org/10.1007/1-4020-3331-1_9
Satake K, Hirata K, Yamaki S, Tanioka Y (2006) Re-estimation of tsunami source of the 1952 Tokachi-oki earthquake. Earth Planets Space 58:535–542. https://doi.org/10.1186/BF03351951
Tanioka Y, Satake K (1996) Tsunami generation by horizontal displacement of ocean bottom. Geophys Res Lett 23:861–864. https://doi.org/10.1029/96GL00736
Tanioka Y, Hirata K, Hino R, Kanazawa T (2004) Detailed slip distribution of the 2003 Tokachi-oki earthquake estimated from tsunami waveforms (in Japanese with english abstract). Zisin 57(2):75–81. https://doi.org/10.4294/zisin1948.57.2_75
Tanioka Y, Hirata K, Hino R, Kanazawa T (2004) Slip distribution of the 2003 Tokachi-oki earthquake estimated from tsunami waveform inversion. Earth Planets Space 56:373–376. https://doi.org/10.1186/BF03353067
Tanioka Y, Nishimura Y, Hirakawa K, Imamura F, Abe I, Abe Y, Shindou K, Matsutomi H, Takahashi T, Imai K, Harada K, Namegawa Y, Hasegawa Y, Hayashi Y, Nanayama F, Kamataki T, Kawata Y, Fukasawa Y, Koshimura S, Hada Y, Azuma Y, Hirata K, Kamikawa A, Yoshikawa A, Shiga T, Kobayashi M, Masaka S (2004) Tsunami run-up heights of the 2003 Tokachi-oki earthquake. Earth Planets Space 56:359–365. https://doi.org/10.1186/BF03353065
Tanioka Y, Nishimura Y, Hirakawa K, Imamura F, Abe I, Abe Y, Shindou K, Matsutomi H, Takahashi T, Imai K, Fujima K, Harada K, F. N, Hasegawa Y, Hayashi Y, Yoshikawa A, Siga T, Kamikawa A, Kobayash M, Masaka S, Kamataki T, Nanayama F, Satake K, Kawata Y, Fukasawa Y, Koshimura S, Hada Y, Azumai Y, Hirata K (2005) Field survey of the 2003 Tokachi-Oki earthquake tsunami and simulation at the Ootsu harbor located at the Pacific Coast of Hokkaido, Japan. In: Satake K (ed) Tsunamis, vol 23. Springer, Dordrecht, pp 135–156, https://doi.org/10.1007/1-4020-3331-1_8
Tanioka Y, Satake K, Hirata K (2007) Recurrence of recent large earthquakes along the Southernmost Kurile-Kamchatka Subduction Zone. In: Eichelberger J, Gordeev E, Izbekov P, Kasahara M, Lees J (Eds) Volcanism and Subduction: The Kamchatka Region vol 172, American Geophysical Union (AGU), pp 145–152. https://doi.org/10.1029/172GM13
Tsushima H, Hino R, Tanioka Y, Imamura F, Fujimoto H (2012) Tsunami waveform inversion incorporating permanent seafloor deformation and its application to tsunami forecasting. J Geophys Res Solid Earth 117:B03311. https://doi.org/10.1029/2011JB008877
Virtanen P, Gommers R, Oliphant TE, Haberland M, Reddy T, Cournapeau D, Burovski E, Peterson P, Weckesser W, Bright J, van der Walt SJ, Brett M, Wilson J, Millman KJ, Mayorov N, Nelson ARJ, Jones E, Kern R, Larson E, Carey CJ, Polat İ, Feng Y, Moore EW, VanderPlas J, Laxalde D, Perktold J, Cimrman R, Henriksen I, Quintero EA, Harris CR, Archibald AM, Ribeiro AH, Pedregosa F, van Mulbregt P (2020) SciPy 1.0: Fundamental algorithms for scientific computing in Python. Nat Methods 17:261–272. https://doi.org/10.1038/s41592-019-0686-2
Watanabe O, Matsumoto H, Sugioka H, Mikada H, Suyehiro K, Otsuka R (2004) Offshore monitoring system records recent earthquake off Japan's northernmost island. Eos Trans Am Geophys Union 85(2):14. https://doi.org/10.1029/2004EO020003
Wessel P, Luis J, Uieda L, Scharroo R, Wobbe F, Smith WH, Tian D (2019) The generic mapping tools version 6. Geochem Geophys Geosystems 20:5556–5564. https://doi.org/10.1029/2019GC008515
Yagi Y (2004) Source rupture process of the 2003 Tokachi-oki earthquake determined by joint inversion of teleseismic body wave and strong ground motion data. Earth Planets Space 56:311–316. https://doi.org/10.1186/BF03353057
Yamanaka Y, Kikuchi M (2003) Source process of the recurrent Tokachi-oki earthquake on September 26, 2003, inferred from teleseismic body waves. Earth Planets Space 55:e21–e24. https://doi.org/10.1186/BF03352479

Publisher's Note